coatings

MDPI

Article

# First-Principles Investigation of Point Defects on the Thermal Conductivity and Mechanical Properties of Aluminum at Room Temperature

**Touwen Fan [1,2], Zixiong Ruan [1], Baohua Nie [2], Yikai Liao [1], Bowen Huang [1], Zimeng Xu [1], Yuanzhi Wu [1,*], Te Hu [2] and Dongchu Chen [2,*]**

[1] Hunan Institute of Technology, College of Science and Research Institute of Automobile Parts Technology, Hengyang 421002, China; fantouwen@hotmail.com (T.F.); ruan_625627@163.com (Z.R.); 18130542074@163.com (Y.L.); w05851211@gmail.com (B.H.); 19118818568@163.com (Z.X.)

[2] School of Material Science and Hydrogen Energy Engineering, Foshan University, Foshan 528001, China; niebaohua@fosu.edu.cn (B.N.); hute98@hotmail.com (T.H.)

* Correspondence: 2013001767@hnit.edu.cn (Y.W.); chendc@fosu.edu.cn (D.C.); Tel.: +0734-3452317 (Y.W.)

**Abstract:** The effects of point defects on the mechanical and thermal conductivity of aluminum at room temperature have been investigated based on the first-principles calculations combined with the Boltzmann equation and the Debye model. The calculated results showed the equilibrium lattice constants $a_0$ of all $RE_{Al}$ are larger than that of Al, and the defective formation energy $E_f$ of all $RE_{Al}$ is lower than that of $V_{Al}$. Both $a_0$ and $E_f$ increase from Sc to La and then decrease linearly to Lu. The effects of solute atoms on the mechanical properties of the Al matrix were further calculated, and compared with Al, it is found that the $RE_{Al}$ defects decrease the elastic constant $C_{ij}$, Cauchy pressure $C_{12}$–$C_{44}$, bulk modulus $B$, shear modulus $G$, Young's modulus $E$, $B/G$ and Poisson's ratio $\nu$ of Al, except for $C_{44}$ of $RE_{Al}$ (RE = La-Nd). With the increase of atomic number, the $C_{11}$ and $E$ of Al-containing $RE_{Al}$ decrease from Sc to La and then slowly increase to Lu, whereas $C_{12}$, $C_{44}$, $B$, and $G$ have little change. Meanwhile, the values of $C_{12}$–$C_{44}$ and $B/G$ of Al-containing $RE_{Al}$ increase from Sc to Ce, and it slightly change after Ce, while $\nu$ is nearly unchanged. All defects containing Al present nonuniform and ductility. Finally, the effects of rare earth (RE) atoms on the thermal conductivity (TC) of Al alloys have been investigated based on the first-principles calculations. The reduction of TC of Al alloys by RE solute atoms $RE_{Al}$ is much greater than that by the $L1_2$ $Al_3RE$ phase with the same concentration of RE, which is in good agreement with the experiments. With the RE atomic number increasing, the total TC $\kappa$ of the Al-RE solid solution decreases from Sc to La firstly and then increases linearly to Lu. Moreover, the decrement of TC $\Delta\kappa$ of the Al matrix by early $RE_{Al}$ (RE = La-Sm) is larger than that by $V_{Al}$, while the later $RE_{Al}$ (RE = Gd-Lu) shows the opposite influence.

**Keywords:** stability; mechanical properties; thermal conductivity; solute atoms; $L1_2$ $Al_3RE$ phase

check for updates

**Citation:** Fan, T.; Ruan, Z.; Nie, B.; Liao, Y.; Huang, B.; Xu, Z.; Wu, Y.; Hu, T.; Chen, D. First-Principles Investigation of Point Defects on the Thermal Conductivity and Mechanical Properties of Aluminum at Room Temperature. *Coatings* **2023**, *13*, 1357. https://doi.org/10.3390/coatings13081357

Academic Editor: Emilio Bellingeri

Received: 20 June 2023
Revised: 20 July 2023
Accepted: 31 July 2023
Published: 2 August 2023

**Copyright:** © 2023 by the authors. Licensee MDPI, Basel, Switzerland. This article is an open access article distributed under the terms and conditions of the Creative Commons Attribution (CC BY) license (https://creativecommons.org/licenses/by/4.0/).

## 1. Introduction

Al-based alloys are widely applied in automotive, aerospace, and electronic industries as they exhibit low density, high specific strength, and welding strength [1–3], and their applications as potential in automobile engines and brakes, gearbox housings, and electronic packaging are increasing, because of their good creep-resistance, high specific strength and high thermal conductivity (TC) [4–10]. In detail, automotive engine blocks and cylinder heads mainly come from hypo-eutectic Al-Si alloys with Mg and Cu, e.g., A356 alloy (Al-7 Si-0.3 Mg), 319 alloy (Al-7 Si-4 Cu), and A380 alloy (Al-9Si-3Cu) [11,12]. Although they are known to have a good tensile strength of the order of ~270~320 MPa, the thermal conductivity within 120 $Wm^{-1}K^{-1}$ is far less than pure Al of 240 $Wm^{-1}K^{-1}$ [13–16]. The

reason mainly comes from the influence of solid solution and particles by adding various micro-alloy elements, especially point defects [15,17].

Point defects that include intrinsic and impurity defects are common in materials and play key roles in the mechanical and thermal performance of Al alloys [18–20]. It is reported that the TC of materials is significantly influenced by the impurities dissolved in [21–23]. Vandersluis et al. reported the reason for the increased TC of the T7 samples of cylinder heads, which was the cast of 319-type Al alloy by heat treatment [16]. They pointed out that the more complete precipitation of $Al_2Cu$ during over-aging was suggested as predominant in improving the TC of the T7 samples by depleting the solute atoms in the Al matrix, which act as electron scattering centers. Very recently, a high-performance Al-Si alloy with TC of 169.34 $Wm^{-1}K^{-1}$ was reported by Weng et al. [24]. They explained that the prominent performance is due to the systematic optimization of micro-structure, e.g., reducing the solute atoms in the primary phase. The addition of rare-earth (RE) elements has become an effective measure to further improve the physical properties of Al-based alloys and thus are widely investigated [25–36]. Liu et al. studied the effect of RE elements on the resistivity of Al wires [37]. Their results showed that when RE elements were added to the Al melt, forming the transitional compounds with impurities Fe and Si, namely, $REFe_2$ and $RESi_2$, respectively, which reduced the amount of impurity elements in the Al solid solution matrix, and thus the TC of 6063 Al alloy has been largely improved.

However, up to now, due to a series of various and extensive experimental workloads, it's difficult to accurately and extensively study the effect of specific factors on thermal conductivity in the experiment [38–40], and most of the research mainly studied the effects of the second phase particles [41–48], and the effects of solute atoms on the stability, mechanical properties, TC of Al matrix are rarely investigated. In addition, the relationship between stability, mechanical properties, TC, and RE atomic number has not been respectively obtained, and the effects of the second phases and RE solute atoms on the TC have not been systematically compared. Fortunately, in recent years, with the improvement of computing power, theoretical calculation, e.g., first-principles calculations, has been widely used in the analysis of various materials [49–58]. Herein, we have calculated the defective formation of impurities and then have analyzed the effects of RE solute atoms and vacancy on TC of the Al matrix; finally, the effects of dissolution of 1% RE, as solute atoms and $L1_2$ $Al_3RE$ second phases, respectively, on the TC of Al matrix has been discussed.

## 2. Computational Detail

In the theoretical framework of density functional theory [59], all calculations within the generalized gradient approximation (GGA) [60] were accomplished in the Vienna ab initio simulation package (VASP) of 5.4.4 version [61], and the projector augmented wave (PAW) potentials [62] were employed for treating the core-valence interactions. In the current calculation, a $3 \times 3 \times 3$ supercell model containing 108 atoms expanded from a stable unit cell, which can be found from work conducted by Liu et al. [48], as shown in Figure 1, was employed for this study. During the execution, the PAW_GGA pseudopotentials of Sc, Y_sv, La, and (Ce-Lu)_3 were used; where _sv and _3 present the electrons with s shell as valence electron and the version of pseudopotentials. The wave energy cut-off of 350 eV was chosen, and the first Brillouin zone sampling was carried out using the Gamma centered Monkhorst–Pack method [63] with $3 \times 3 \times 3$ k-point mesh for the warrant of high accuracy. The convergence criterion for total energy and Hellman-Feymann forces [64] was established until the values reached $10^{-6}$ eV and 0.01 eV/Å, respectively, to stop the calculation.

Based on the energy strain method, the elastic constant $C_{ij}$ carried out in the VASPKIT code [65] is calculated with the same accuracy as above. Solving the Boltzmann transport equation (BTE), the electronic transport properties of defective compounds, including perfect supercells, were further studied, performing in the BoltzTraP2 code [66], and a larger k-mesh with $6 \times 6 \times 6$ and cut-off energy of plane wave basis of 500 eV was used to calculate electronic transport properties.

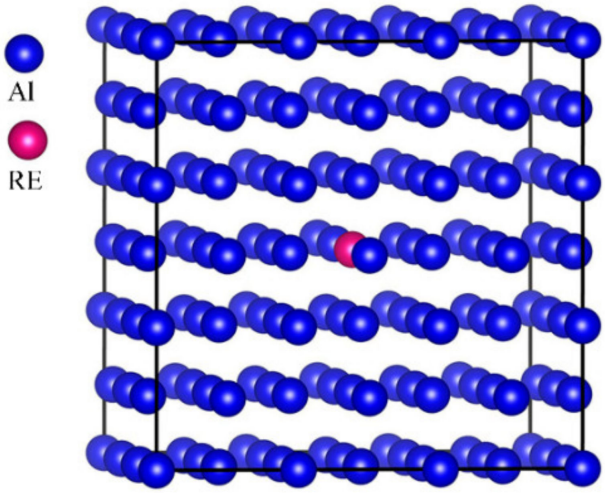



**Figure 1.** The defects model of $RE_{Al}$ in Al matrix.

## 3. Result and Discussion

### *3.1. Defective Formation Energy*

In the system of Al, two types of point defects containing vacancies $V_{Al}$ and impurity elements replacing the Al atom in the lattice $X_{Al}$ are necessary to investigate, as they generally occur in Al. Here, an evaluation for the stability of these defects is considered, as the following expression [67,68]:

$$E_f = E_{def} - E_{per} - \sum_i n_i \mu_i \quad (1)$$

where $E_{def}$ and $E_{per}$ are the total energies of the defective-containing and perfect supercells, respectively. $n_i$ is the number of atoms increased ($n_i > 0$) or deleted ($n_i < 0$), and $\mu_i$ is the corresponding chemical potential of specific species, respectively. Further, to avoid the occurrence of precipitate of solid, the chemical potential $\mu_i$ in defective phases should be less than the chemical potential of bulk $\mu_{bulk}$.

$$\mu_i - \mu_{bulk} \leq 0 \quad (2)$$

To study the effects of point defects on the mechanical and thermal conductivity of aluminum, the lattice constant $a_0$ of Al bulk and $E_f$ of 18 defectives are first calculated, and the results are summarized in Table 1. It can be seen that the lattice constant $a_0$ of Al bulk and defective formation energy $E_f$ of $V_{Al}$ are in good agreement with experiment values and other theoretical predictions [69–72], and the errors are not more than 1.36% and 16.45%, respectively. Furthermore, to illustrate the potential relation between the $a_0$ and $E_f$ of rare elements substitution $RE_{Al}$ and the atomic number, the $a_0$, and $E_f$ as a function of atomic number of RE are depicted in Figure 2a,b. Clearly, it is seen that the equilibrium lattice constants $a_0$ of Al-$RE_{Al}$ is larger than that of Al of 4.038 Å as RE solute atoms force lattice distortion, and it increases from 4.045 Å for Sc to 4.061 Å for La firstly and then decreases linearly to 4.049 Å for Lu. One can see that the $E_f$ of all $RE_{Al}$ is lower than that of $V_{Al}$, indicating that the impurity atoms are easier to replace the Al site than Al escaping the Al matrix. The results further show that with the increase of atomic number, the $E_f$ of $RE_{Al}$ increases from −1.062 eV for Sc to 0.316 eV for La at first and then decreases linearly to −0.641 eV for Lu, and the $Sc_{Al}$ has the lowest $E_f$. The phenomenon shows the Sc element has larger solubility than other RE elements in the Al matrix, which is in agreement well with the results of the experiment and theoretical data of Zhang et al. [28,73,74].

**Table 1.** The calculated equilibrium lattice constants $a_0$ (Å) and defective formation energy $E_f$ (eV) in Al.

| Def. | $a_0$ | $E_f$ |
|---|---|---|
| Al | 4.038; 4.039 [69]; 3.983 [69]; 4.032 [70] | - |
| $V_{Al}$ | 4.034 | 0.626; 0.665 [69]; 0.729 [69]; 0.670 [71] 0.540 [72]; 0.700 [72] |
| $Sc_{Al}$ | 4.045 | −1.062 |
| $Y_{Al}$ | 4.052 | −0.507 |
| $La_{Al}$ | 4.061 | 0.316 |
| $Ce_{Al}$ | 4.060 | 0.314 |
| $Pr_{Al}$ | 4.059 | 0.137 |
| $Nd_{Al}$ | 4.058 | −0.004 |
| $Pm_{Al}$ | 4.057 | −0.140 |
| $Sm_{Al}$ | 4.055 | −0.219 |
| $Eu_{Al}$ | 4.055 | −0.316 |
| $Gd_{Al}$ | 4.054 | −0.402 |
| $Tb_{Al}$ | 4.054 | −0.463 |
| $Dy_{Al}$ | 4.051 | −0.513 |
| $Ho_{Al}$ | 4.051 | −0.551 |
| $Er_{Al}$ | 4.050 | −0.584 |
| $Tm_{Al}$ | 4.050 | −0.604 |
| $Yb_{Al}$ | 4.050 | −0.633 |
| $Lu_{Al}$ | 4.049 | −0.641 |

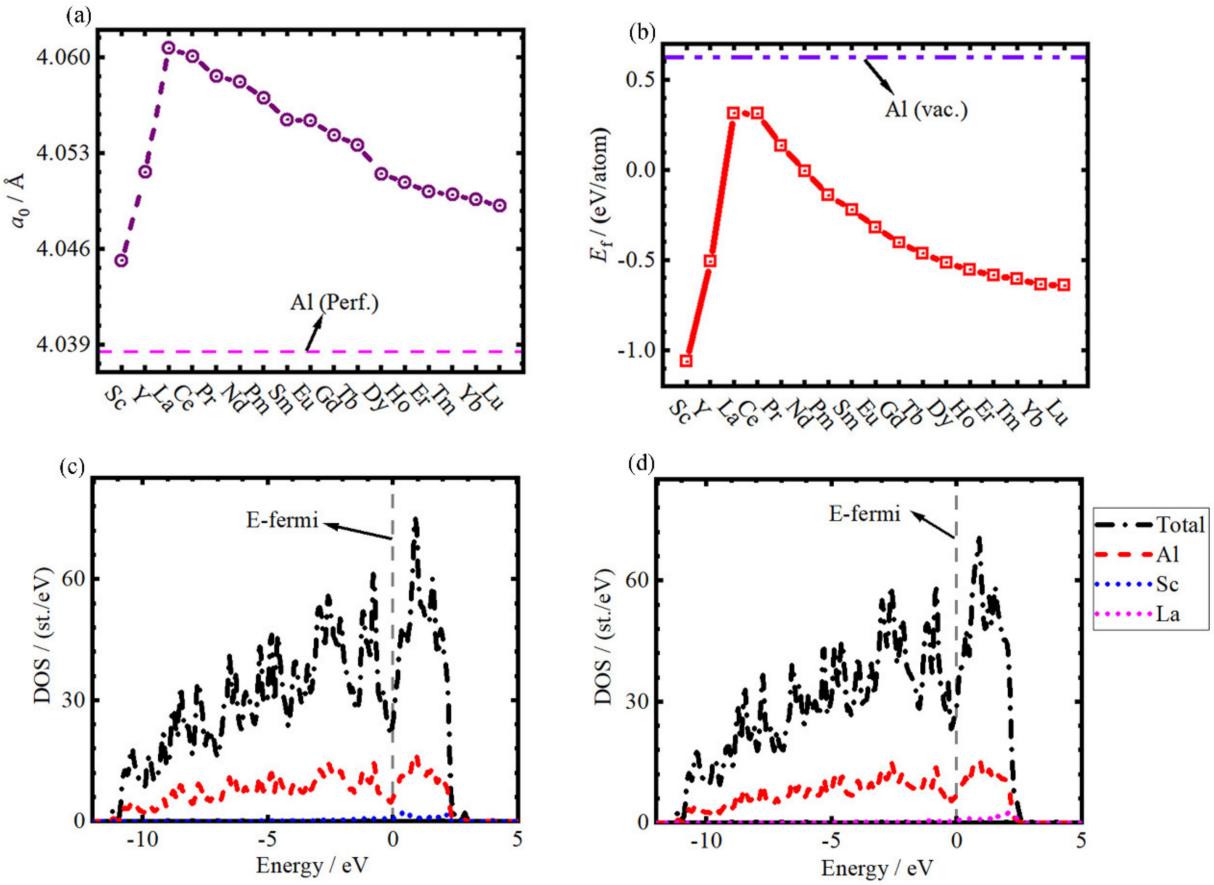



**Figure 2.** (**a**) The $a_0$ and (**b**) $E_f$ of defects as a function of atomic number. (**c**,**d**) The DOSs for $Sc_{Al}$ and $La_{Al}$.

To investigate the underlying physical mechanisms of $RE_{Al}$ defects on the properties of the Al matrix, the electron structures are calculated, and the obtained density of states (DOSs) for $Sc_{Al}$ and $La_{Al}$, presenting the best and the worst stability, respectively, are shown in Figure 2. As can be seen from Figure 2c,d, the addition of Sc results in higher peaks near the Fermi level compared to that of the addition of La, implying that the effect of a chemical bond between Sc and Al atoms is larger. This phenomenon shows the stronger Al-Sc bond, and the defect $Sc_{Al}$ is more stable than $La_{Al}$.

### *3.2. Mechanical Properties*

The bulk modulus $B$, shear modulus $G$, Young's modulus $E$ and Poisson's ratio $\nu$ determined by [75] the elastic constants $C_{ij}$ are important family members of mechanical parameters. The $C_{ij}$ are calculated from the energy-strain relationship by adding small strains to the original optimization lattice ordering, and the energy-strain relation $\Delta E\ (V, \{\varepsilon_i\})$ of material under the quadratic function is given by [65,76]:

$$\Delta E_{(V,\{\varepsilon_i\})} = E_{stain}(V, \{\varepsilon_i\}) - E_0(V_0, 0) = \frac{V_0}{2}\sum_{i,j=1}^{6} C_{ij}\varepsilon_i\varepsilon_j \quad (3)$$

where $E_{stain}(V, \{\varepsilon_i\})$ and $E_0(V_0, 0)$ are the total energies of the strained-lattice $V$ and equilibrium at the volume of $V_0$, respectively.

In Born stability criteria, determining the mechanical stability for a Cubic crystal system is as following formulas [48,77,78]:

$$C_{11} > 0, C_{44} > 0, C_{11} - C_{12} > 0, C_{11} + 2C_{12} > 0 \quad (4)$$

The bulk modulus $B$ can be used to evaluate the ability to resist volume deformation and strength of the average atomic bond, and the shear modulus $G$ can describe the resistant of the materials from shape-changing [79], and both are used to estimate the Vickers' hardness of materials according to $H_v = 2(KG)^{0.585} - 3$ [80,81], where $K = G/B$. And the Young's modulus $E$ mainly demonstrates the detailed value of the tensile strength of materials. They can be calculated by the elastic constant matrix according to Voigt-Reuss-Hill's theory, which can be obtained as follows [48,82–86]:

$$B_v = B_R = B = \frac{C_{11} + 2C_{12}}{3} \quad (5)$$

$$G_v = \frac{C_{11} - C_{12} + 3C_{44}}{5} \quad (6)$$

$$G_R = \frac{5 \times (C_{11} - C_{12}) \times C_{44}}{4 \times C_{44} + 3 \times (C_{11} - C_{12})} \quad (7)$$

$$G = \frac{G_V + G_R}{2} \quad (8)$$

The Young's modulus $E$ and Poisson's ratio $\nu$ can be given by refs. [87–89]:

$$E = \frac{9GB}{3B + G},\ \nu = \frac{3B - 2G}{2 \times (3B + G)} \quad (9)$$

where $G_V$, $B_V$ and $G_R$, $B_R$ are the shear and bulk moduli of Voigt and Reuss approximations, respectively.

The calculated values with the experimental data and previously computed results are presented in Table 2. A good coincidence can be clearly identified, and the difference between the computed values and the experiment data is within 10%. It can be found that compared with Al, the parameters involving $C_{11}$, $C_{12}$, $C_{12}$–$C_{44}$ $B$, $G$, $E$ $B/G$, and ν of all defective supercell decrease while $C_{44}$ increases, except for $RE_{Al}$ (RE = La-Nd). Fur-

thermore, it can be seen that all situations meet the mechanical stability criteria according to Equation (4). To study the variation regulation of mechanical parameters, the $C_{11}$, $C_{12}$, $C_{44}$, $C_{12}$–$C_{44}$ $B$, $G$, $E$ $B/G$, and ν of $RE_{Al}$-containing Al with the variation of the atomic number of RE are further illustrated in Figure 3. A clear result seen in Figure 3a shows that the $C_{11}$ of $RE_{Al}$ decreases from 96.02 GPa for Sc to 91.05 GPa for La and slowly increases to 94.07 Ga for Lu, while there is a little variation for $C_{12}$ and $C_{44}$. The $B$, $G$, and $E$ of $RE_{Al}$ are described in Figure 3b. The same law as $C_{11}$ can be seen in that the $E$ decreases from 80.48 GPa for Sc to 78.28 GPa for Y and slowly increases to 79.57 GPa for Lu with the increase of atomic number, while $B$ and $G$ have little change.

**Table 2.** The calculated elastic constants (units in GPa), bulk modulus $B$, shear modulus $G$, Young's modulus $E$, Poisson's ratio $\nu$, and $B/G$ of $RE_{Al}$ containing the perfect supercell and unit cell.

| Systems | $C_{11}$ | $C_{12}$ | $C_{44}$ | $C_{12}$–$C_{44}$ | $B$ | $G$ | $E$ | $B/G$ | $\nu$ |
|---|---|---|---|---|---|---|---|---|---|
| Al | 121.05 | 63.64 | 34.50 | 29.14 | 82.78 | 32.05 | 85.16 | 2.583 | 0.329 |
| Al * | 110.47 | 67.33 | 33.94 | 33.39 | 81.71 | 28.30 | 76.11 | 2.887 | 0.345 |
| | 107.00 [a] | 61.00 [a] | 28.00 [a] | 28.78 [b] | 76.73 [b] | 28.59 [b] | 76.30 [b] | 2.68 [b] | 0.33 [b] |
| | 109.98 [b] | 60.11 [b] | 31.33 [b] | | | | | | |
| $V_{Al}$ | 93.71 | 43.19 | 35.45 | 7.74 | 60.03 | 30.95 | 79.24 | 1.939 | 0.280 |
| $Sc_{Al}$ | 96.02 | 42.33 | 35.06 | 7.27 | 60.23 | 31.51 | 80.48 | 1.912 | 0.277 |
| $Y_{Al}$ | 93.18 | 43.26 | 34.93 | 8.34 | 59.90 | 30.53 | 78.28 | 1.962 | 0.282 |
| $La_{Al}$ | 91.05 | 43.14 | 33.98 | 9.16 | 59.11 | 29.54 | 75.96 | 2.001 | 0.286 |
| $Ce_{Al}$ | 91.18 s | 43.29 | 33.99 | 9.31 | 59.26 | 29.54 | 75.99 | 2.006 | 0.286 |
| $Pr_{Al}$ | 91.72 | 42.84 | 34.23 | 8.61 | 59.13 | 29.91 | 76.78 | 1.977 | 0.284 |
| $Nd_{Al}$ | 91.45 | 43.29 | 34.25 | 9.04 | 59.34 | 29.74 | 76.45 | 1.995 | 0.285 |
| $Pm_{Al}$ | 91.75 | 43.28 | 34.40 | 8.88 | 59.44 | 29.90 | 76.81 | 1.988 | 0.285 |
| $Sm_{Al}$ | 92.23 | 43.30 | 34.59 | 8.71 | 59.61 | 30.11 | 77.31 | 1.980 | 0.284 |
| $Eu_{Al}$ | 92.37 | 43.20 | 34.59 | 8.61 | 59.59 | 30.17 | 77.44 | 1.975 | 0.283 |
| $Gd_{Al}$ | 92.01 | 43.60 | 34.68 | 8.92 | 59.74 | 30.03 | 77.15 | 1.990 | 0.285 |
| $Tb_{Al}$ | 92.96 | 43.06 | 34.74 | 8.33 | 59.70 | 30.42 | 78.02 | 1.962 | 0.282 |
| $Dy_{Al}$ | 93.10 | 43.37 | 34.98 | 8.39 | 59.95 | 30.51 | 78.26 | 1.965 | 0.282 |
| $Ho_{Al}$ | 93.88 | 43.05 | 35.03 | 8.02 | 59.99 | 30.80 | 78.91 | 1.947 | 0.281 |
| $Er_{Al}$ | 94.14 | 42.99 | 35.08 | 7.91 | 60.04 | 30.91 | 79.14 | 1.943 | 0.280 |
| $Tm_{Al}$ | 94.29 | 42.90 | 35.07 | 7.83 | 60.03 | 30.96 | 79.26 | 1.939 | 0.280 |
| $Yb_{Al}$ | 94.48 | 42.80 | 35.06 | 7.74 | 60.03 | 31.03 | 79.40 | 1.935 | 0.280 |
| $Lu_{Al}$ | 94.67 | 42.73 | 35.09 | 7.65 | 60.04 | 31.10 | 79.57 | 1.931 | 0.279 |

* Experimental values. [a] Ref. [90] and [b] Ref. [48] represent the results of the experiment at 175 K and GGA-PBE calculation at 0 K, respectively.

To study the influence of solute atoms on the characteristics of bonds, we have calculated the Cauchy pressure $C_{12} - C_{44}$, which is a critical index to describe the directional chemical bonding features of materials [91]. It is proved that the atomic bonds have metallic characteristic if $C_{12} - C_{44} > 0$, while those satisfying $C_{12} - C_{44} < 0$ has directional covalent bonds, and the larger absolute value shows the stronger bonding characteristic of materials for both cases [92,93]. Figure 3c shows the change of $C_{12} - C_{44}$ with the increased atomic number, and the dissolution of all RE elements leads to a significant decrease in Cauchy pressure with a minimum of 68.05%, indicating the dissolution of RE elements in the Al matrix reduces the metallic characteristic of atomic bonding. Meanwhile, it is found that the values of $C_{12} - C_{44}$ of defects increase from Sc to Ce, and it slightly change after Ce. The Poisson's ratio $\nu$ is usually used to judge the heterogeneity of materials [94], and greater/smaller $\nu$ than the critical value of 0.26 is an implication of uniform/nonuniform strain response to exerted stress, respectively. The Pugh's ratio $B/G$ relates mainly to the plasticity of materials, and a higher/lower $B/G$ than the critical value of 1.75 [48] leads to the ductile/brittle behavior of materials, respectively. The calculated $\nu$ and $B/G$ of $RE_{Al}$ with the increases of atomic number, as shown in Figure 3d. It is seen that the $\nu$ and $B/G$ of defects range from ~0.286 to ~2.006, respectively. The $B/G$ shows the same trend compared

to $C_{12}$-$C_{44}$ with the increase of atomic number while $\nu$ is unchanged. Moreover, all defects containing perfect supercells present nonuniform and ductility.

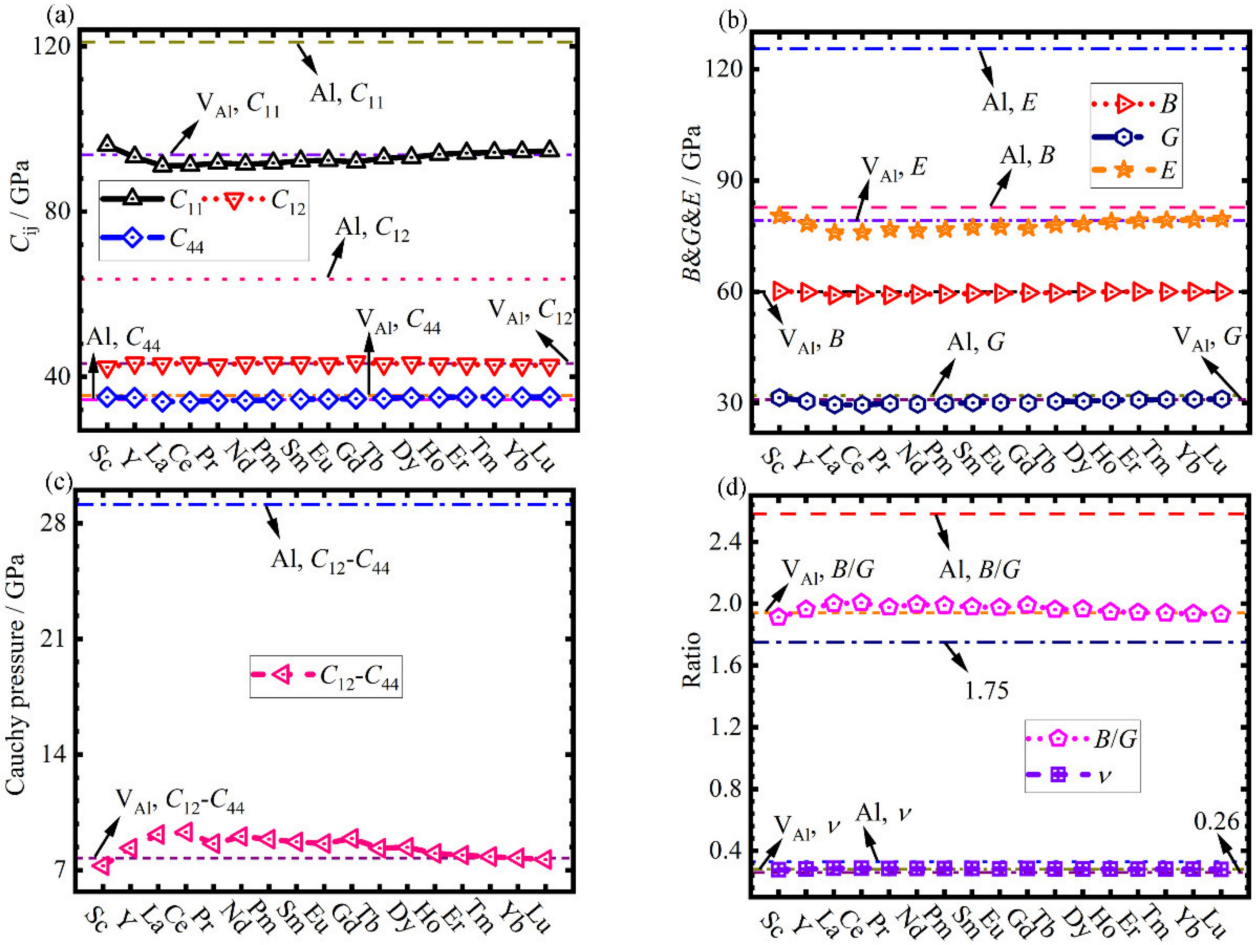



**Figure 3.** (**a**) The elastic constants $C_{ij}$, (**b**) $B$, $G$, and $E$ of defects, (**c**) Cauchy pressure $C_{12} - C_{44}$, and (**d**) the Pugh's ratio $B/G$ and Poisson's ratio $\nu$ as a function of atomic number.

### *3.3. Thermal Conductivity*

The power system in modern electrical equipment needs materials possessing high thermal conductivity (TC) for dissipating heat faster so as to prolong its life and improve its operation efficiency [95,96]. The TC of an objective usually contains two aspects; the first one comes from the lattice TC (LTC) $\kappa_l$, and the other one originates from the electronic TC (ETC) $\kappa_e$. That is to say, the total thermal conductivity $\kappa = \kappa_e + \kappa_l$. For pure metal and their compounds, heat transfer mainly involves the heat exchange between electrons. Then, we have firstly calculated the $\kappa_e$ by using the Wiedemann–Franz law [97], $\kappa_e = L\sigma T$, where $L = \frac{\pi^2 \kappa_B^2}{3e^2}$ denotes the Lorentz number, $\sigma$ and $T$ represent the electrical conductivity and temperature in Kelvins, respectively. Here, the $\sigma$ of materials are further obtained by using Boltzmann transport theory [98–101], and it's given by the following formula:

$$\sigma_{\alpha\beta}(T,\mu) = \frac{1}{\Omega}\int \sigma_{\alpha\beta}(\varepsilon)\left[-\frac{\partial f_0(T,\varepsilon,\mu)}{\partial \varepsilon}\right]d\varepsilon \quad (10)$$

where $e$, $\mu$, and $\varepsilon$ are the electronic charge, the band-energy, and the chemical potential, respectively. And the core of Equation (10) is the tensor $\sigma_{\alpha\beta}$, which mainly indicates

the energy projected transport distribution function and contains the system-dependent information, which is computed as follows:

$$\sigma_{\alpha\beta}(\varepsilon) = \frac{e^2}{N}\sum_{i,K}\tau_{i,k}\nu_{\alpha}(i,K)\nu_{\beta}(i,K)\frac{\delta(\varepsilon-\varepsilon_{i,K})}{d\varepsilon} \quad (11)$$

where $N$, $i$, $K$, and $\nu_{\alpha,\beta}(i, K)$ are the number of k-points, the band index, the wave vector, and the group velocity of the acoustic wave, respectively. Equation (10) is settled from constant relaxation time approximation (RTA) [98,99]. For convenience, in the present work, we used a common relaxation time for metal Al of $10^{-13}$ s. The energy limit of the system is set to be 0.30 Ry for the chemical potential around the Fermi level [99].

We have further calculated the $\kappa_l$, which is solved by two key parameters: Debye temperature $\theta_\alpha$ and Grüneisen parameter $\gamma$, using the Slack equation:

$$\kappa_l(\theta_\alpha) = \frac{0.849\times 3\sqrt[3]{(4)}}{20\pi^3(1-0.154\gamma^{-1}+0.228\gamma^{-2})}\times\left(\frac{\kappa_B\theta_\alpha}{\hbar}\right)^2\frac{\kappa_B M_{av}V^{\frac{1}{3}}}{\hbar\gamma^2} \quad (12)$$

and

$$\kappa_l(T) = \kappa_l(\theta_\alpha)\frac{\theta_\alpha}{T} \quad (13)$$

where $V$, $M_{av}$ $\kappa_B$, and $\hbar$ are the primitive cell volume, average atomic mass, Boltzmann constant, and Reduced Planck constant, respectively.

The ETC $\kappa_e$ of all defects-containing Al supercell at 300 K is calculated first, and the obtained results as a function of the atomic number of RE are drawn in Figure 4a. The $\kappa_e$ value of 208 $Wm^{-1}K^{-1}$ for pure Al is in good agreement with the calculation value of 186.10 $Wm^{-1}K^{-1}$ at a room temperature of 300 K by Wen et al. [102]. A clear law can be seen that the $\kappa_e$ of Al with $RE_{Al}$ varies with the atomic number of RE, it decreases from 153.23 $Wm^{-1}K^{-1}$ for Sc to 128.34 $Wm^{-1}K^{-1}$ for La at first and then increases linearly to 153.73 $Wm^{-1}K^{-1}$ for Lu, and the $\kappa_e$ of Al with $RE_{Al}$ is greatly reduced as compared to that of pure Al, the decrements percent ranges from 24% to 38%. Moreover, the $\kappa_e$ of Al with early RE (La-Sm) solute atom is lower than that with $V_{Al}$, while later RE (Gd-Lu) replacing Al shows the opposite influence. The LTC $\kappa_l$ of Al with $RE_{Al}$ as a function of atomic number at 300 K has been further computed, and the results are elucidated in Figure 4b. It can be seen that the calculated LTC $\kappa_l$ of 9.82 $Wm^{-1}K^{-1}$ for Al in this work is in good agreement with the calculated value of 4.80 $Wm^{-1}K^{-1}$ by Wen et al. [102]. And the LTC $\kappa_l$ of Al with $RE_{Al}$ decreases slightly from Sc to Y and then nearly unchanged. The maximum loss of $\kappa_l$ of the Al matrix by Sm solute is only 0.53 $Wm^{-1}K^{-1}$. For the $V_{Al}$, the loss of $\kappa_l$ in the Al matrix is also small, ~0.33 $Wm^{-1}K^{-1}$.

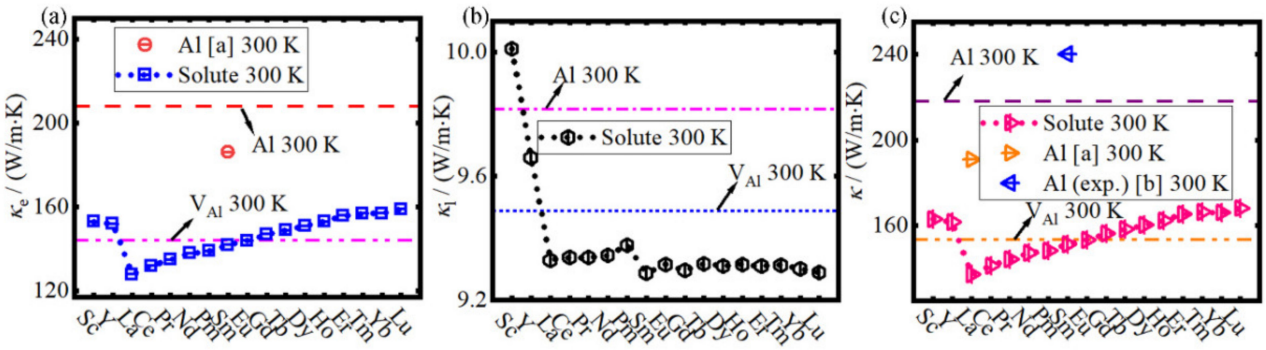



**Figure 4.** (**a**) The calculated the electronic thermal conductivity $\kappa_e$, (**b**) lattice thermal conductivity $\kappa_l$, and (**c**) total thermal conductivity $\kappa$ as a function of atomic number at 300 K.

Based on the calculation of the above two parts, we have computed the total TC $\kappa$ of defective supercells, and the obtained values as a function of the atomic number of

RE are depicted in Figure 4c; a very consistent can be clearly ascertained as compared with both theoretical and experimental values [102,103]. It is found that the total TC $\kappa$ of Al is greatly reduced by the RE solute atom; with the increase of the atomic number of RE, it decreases from 163.01 $Wm^{-1}K^{-1}$ for Sc to 137.33 $Wm^{-1}K^{-1}$ for La firstly and then increases linearly to 168.29 $Wm^{-1}K^{-1}$ for Lu. The total TC $\kappa$ of the Al matrix with early stage $RE_{Al}$ (RE = La-Sm) is lower than that with $V_{Al}$, which is denoted by an orange horizontal dot-dot-dashed line, while the total TC $\kappa$ of the Al matrix with $Sc_{Al}$, $Y_{Al}$, and later stage $RE_{Al}$ (RE = Gd-Lu) possesses higher value.

To quantitatively analyze the different effects between second phase particles ($L1_2$ $Al_3RE$ phases) and RE solute atom on the total TC $\kappa$ of the Al matrix, we have calculated the effects of adding 1% RE at 300 K in the Al matrix for both cases, and the results are shown in Figure 5. It can be seen that for the effect of solute atoms, the reduction of total TC $\kappa$ of the Al matrix increases from 27.17% for Sc to 39.91% for La firstly and then decreases linearly to 24.57% for Lu. Whereas the reduction of the total TC $\kappa$ of the Al matrix by $L1_2$ $Al_3RE$ second phases increases from 1.50% for Sc to 3.43% for La and then slightly decreases to 2.21% for Lu. In short, the influence of RE solute atoms on the TC of Al is much greater than that of $L1_2$ $Al_3RE$ phase particles.

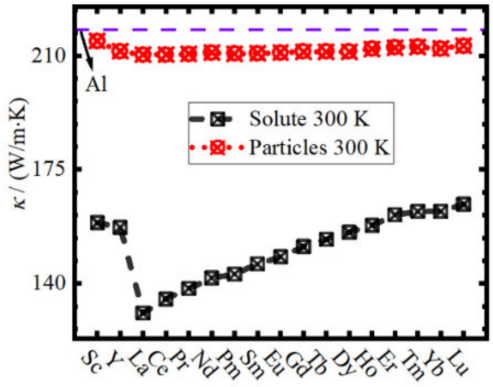



**Figure 5.** The calculated total TC $\kappa$ of the Al matrix by adding 1% second phase particles ($L1_2$ $Al_3RE$ phases) and RE solute atom as a function of the atomic number of RE at 300 K.

## 4. Conclusions

In summary, the effects of point defects on the thermal conductivity of aluminum are studied based on the first principles calculations. The main obtained results are as follows:

(1) The equilibrium lattice constant $a_0$ of $RE_{Al}$ is larger than that of Al, and it increases from Sc to La and linearly decreases to Lu with the increase of atomic number.

(2) The defective formation energy $E_f$ of all $RE_{Al}$ is lower than that of $V_{Al}$, and with the increase of the atomic number of RE, they increase from Sc to La at first and then decrease linearly to Lu.

(3) Compared with Al, the elastic constant $C_{ij}$, Cauchy pressure $C_{12}$-$C_{44}$, bulk modulus $B$, shear modulus $G$, Young's modulus $E$, $B/G$, and Poisson's ratio $\nu$ of all $RE_{Al}$ decrease except for $C_{44}$ of $RE_{Al}$ (RE = La-Nd); With the increase of atomic number, the $C_{11}$ and $E$ of $RE_{Al}$ decreases from Sc to La and slowly increases to Lu while $C_{12}$, $C_{44}$, $B$ and $G$ have little change.

(4) The values of $C_{12} - C_{44}$ and $B/G$ of defects increase Sc to Ce with the increase of atomic number, and it slightly change after Ce, while $\nu$ is unchanged. All defects containing perfect supercells present nonuniform and ductility.

(5) The total TC $\kappa$ is greatly reduced by the RE solute atom in the Al matrix, and it decreases Sc to La firstly and then increases linearly to Lu. The total TC $\kappa$ of the Al matrix with early stage $RE_{Al}$ (RE = La-Sm) is lower than that with $V_{Al}$, while the total TC $\kappa$ of the Al matrix with $Sc_{Al}$, $Y_{Al}$, and later stage $RE_{Al}$ (RE = Gd-Lu) possesses a higher value.

(6) When 1% RE atoms are added to the Al matrix, the reduction of TC by RE solute atoms is much greater than that by the formation of the $L1_2$ $Al_3RE$ second phase.

**Author Contributions:** Methodology, T.F. and Z.R.; validation, T.F. and Y.W.; investigation, T.F., Z.R. and T.H.; resources, T.F., Y.L., B.H., Z.X., Y.W. and D.C.; data curation, T.F., B.N., Y.L., B.H., Z.X., Y.W. and D.C.; writing—original draft, Z.R.; writing—review & editing, T.F., T.H. and Z.R.; visualization, Z.R.; Project administration, T.F., Y.W. and D.C. All authors have read and agreed to the published version of the manuscript.

**Funding:** This work is supported by the R & D plan for key areas in Guangdong Province (2020B010186001, 2020B1515120093), the Scientific Research Project of Hunan Institute of Technology (HQ21016, 21A0564, HP21047, 2022SE090), and the Natural Science Foundation of China (No. 52171115).

**Institutional Review Board Statement:** Not applicable.

**Informed Consent Statement:** Not applicable.

**Data Availability Statement:** Not applicable.

**Acknowledgments:** Calculations performed in this work totally used the Xiangqing High Performance Super Computer System (XHPSCS) and Fanxing Fast Network Program (FFNP), which is supported by the above fundings.

**Conflicts of Interest:** The authors declare no conflict of interest.

## References

1. Wen, K.; Xiong, B.Q.; Fan, Y.Q.; Zhang, Y.A.; Li, Z.H.; Li, X.W.; Wang, F.; Liu, H.W. Transformation and dissolution of second phases during solution treatment of an Al-Zn-Mg-Cu alloy containing high zinc. *Rare Met.* **2018**, *37*, 376–380. [CrossRef]
2. Seidman, D.N.; Marquis, E.A.; Dunand, D.C. Precipitation strengthening at ambient and elevated temperatures of heat-treatable Al(Sc) alloys. *Acta Mater.* **2002**, *50*, 4021–4035. [CrossRef]
3. Czerwinski, F. Thermal Stability of Aluminum Alloys. *Materials* **2020**, *13*, 3441. [CrossRef] [PubMed]
4. Senkov, O.N.; Shagiev, M.R.; Senkova, S.V.; Miracle, D.B. Precipitation of $Al_3$(Sc, Zr) particles in an Al–Zn–Mg–Cu–Sc–Zr alloy during conventional solution heat treatment and its effect on tensile properties. *Acta Mater.* **2008**, *56*, 3723–3738. [CrossRef]
5. Kim, C.W.; Cho, J.I.; Choi, S.W.; Kim, Y.C. The Effect of Alloying Elements on Thermal Conductivity of Aluminum Alloys in High Pressure Die Casting. *Adv. Mater. Res.* **2013**, *813*, 175–178. [CrossRef]
6. Wu, J.; Zhang, H.; Yang, Z.; Li, J.; Wang, X. Effect of copper content on the thermal conductivity and thermal expansion of Al–Cu/diamond composites. *Mater. Des.* **2012**, *39*, 87–92. [CrossRef]
7. Kasprzak, W.; Sahoo, M.; Sokolowski, J.H.; Yamagata, H.; Kurita, H. The Effect of the Melt Temperature and the Cooling Rate on the Microstructure of the Al-20% Si Alloy Used for Monolithic Engine Blocks. *Int. J. Metalcast.* **2009**, *3*, 55–71. [CrossRef]
8. Yu, S.; Wang, R.; Peng, C.; Cai, Z.; Wu, X.; Feng, Y.; Wang, X. Effect of minor scandium addition on the microstructure and properties of Al–50Si alloys for electronic packaging. *J. Mater. Sci.-Mater. El.* **2019**, *30*, 20770–20777. [CrossRef]
9. Deng, J.; Chen, C.; Liu, X.; Li, Y.; Guo, S. A high-strength heat-resistant Al-5.7Ni eutectic alloy with spherical $Al_3Ni$ nano-particles by selective laser melting. *Scripta Mater.* **2021**, *203*, 114034. [CrossRef]
10. Khaki-Davoudi, S.; Nourouzi, S.; Aval, H.J. Microstructure and mechanical properties of AA7075/$Al_3Ni$ composites produced by compocasting. *Mater. Today Commun.* **2021**, *28*, 102537. [CrossRef]
11. Choi, S.W.; Cho, H.S.; Kang, C.S.; Kumai, S. Precipitation dependence of thermal properties for Al-Si-Mg-Cu-(Ti) alloy with various heat treatment. *J. Alloys Compd.* **2015**, *647*, 1091–1097. [CrossRef]
12. Karamouz, M.; Azarbarmas, M.; Emamy, M.; Alipour, M. Microstructure, hardness and tensile properties of A380 aluminum alloy with and without Li additions. *Mater. Sci. Eng. A* **2013**, *582*, 409–414. [CrossRef]
13. Han, Y.; Samuel, A.M.; Doty, H.W.; Valtierra, S.; Samuel, F.H. Optimizing the tensile properties of Al–Si–Cu–Mg 319-type alloys: Role of solution heat treatment. *Mater. Des.* **2014**, *58*, 426–438. [CrossRef]
14. Lumley, R.N.; O'Donnell, R.G.; Gunasegaram, D.R.; Givord, M. Heat treatment of high-pressure die castings. *Metall. Mater. Trans. A* **2007**, *38*, 2564–2574. [CrossRef]
15. Lumley, R.N.; Deeva, N.; Larsen, R.; Gembarovic, J.; Freeman, J. The role of alloy composition and T7 heat treatment in enhancing thermal conductivity of aluminum high pressure diecastings. *Metall. Mater. Trans. A* **2013**, *44*, 1074–1086. [CrossRef]
16. Vandersluis, E.; Lombardi, A.; Ravindran, C.; Bois-Brochu, A.; Chiesa, F.; Mackay, R. Factors influencing thermal conductivity and mechanical properties in 319 Al alloy cylinder heads. *Mater. Sci. Eng. A* **2015**, *648*, 401–411. [CrossRef]
17. Rauta, V.; Cingi, C.; Orkas, J. Effect of annealing and metallurgical treatments on thermal conductivity of aluminium alloys. *Int. J. Metalcast.* **2016**, *10*, 157–171. [CrossRef]

18. Sheng, B.; Niu, M.; Shao, X. Conductivity and magnetic properties study on doped semiconductor material of 3C-SiC: A first-principle investigation. In Proceedings of the IEEE International Conference on Electric Information and Control Engineering 2011, Wuhan, China, 15–17 April 2011; pp. 5758–5761.
19. Majid, A.; Rani, N.; Khan, U.D.; Almutairi, Z.A. First principles study of structural, electronic and magnetic properties of transition metals doped SiC monolayers for applications in spintronics. *J. Magn. Magn. Mater.* **2020**, *503*, 166648. [CrossRef]
20. Cao, Z.; Jin, N.; Ye, J.; Du, X.; Liu, Y. First-principles study on the effects of N and Al doping on the mechanical properties and electronic structures of TiC. *RSC Adv.* **2020**, *10*, 36295–36302. [CrossRef]
21. Li, C.C.; Ren, W.L.; Zhang, L.T.; Ito, K.; Wu, J.S. Effects of Al doping on the thermoelectric performance of CoSi single crystal. *J. Appl. Phys.* **2005**, *98*, 774. [CrossRef]
22. Rajasekar, P.; Umarji, A.M. Effect of Al-doping on suppression of thermal conductivity in Si dispersed β-$FeSi_2$. *Intermetallics* **2017**, *89*, 57–64. [CrossRef]
23. Jia, P.-Z.; Xie, J.-P.; Chen, X.-K.; Zhang, Y.; Yu, X.; Zeng, Y.-J.; Xie, Z.-X.; Deng, Y.-X.; Zhou, W.-X. Recent progress of two-dimensional heterostructures for thermoelectric applications. *J. Phys. Condens. Matter* **2023**, *35*, 073001. [CrossRef] [PubMed]
24. Weng, W.; Nagaumi, H.; Sheng, X.; Fan, W.; Chen, X.; Wang, X. Influence of Silicon Phase Particles on the Thermal Conductivity of Al-Si Alloys. In *Light Metals 2019*; Springer: Berlin/Heidelberg, Germany, 2019; pp. 193–198.
25. Cho, Y.H.; Kim, H.W.; Lee, J.M.; Kim, M.S. A new approach to the design of a low Si-added Al–Si casting alloy for optimising thermal conductivity and fluidity. *J. Mater. Sci.* **2015**, *50*, 7271–7281. [CrossRef]
26. Vlach, M.; Čížek, J.; Smola, B.; Melikhova, O.; Vlček, M.; Kodetová, V.; Kudrnová, H.; Hruška, P. Heat treatment and age hardening of Al–Si–Mg–Mn commercial alloy with addition of Sc and Zr. *Mater. Charact.* **2017**, *129*, 1–8. [CrossRef]
27. Zhang, X.; Wei, J. First-principles investigations on vibrational, thermodynamic, mechanical properties and thermal conductivity of $L1_2$ $Al_3X$ (X=Sc, Er, Tm, Yb) intermetallics. *Phys. Scr.* **2015**, *90*, 1351–1354. [CrossRef]
28. Zhang, X.D.; Wang, S.Q. First-principles study of thermodynamic properties and solubility of aluminum-rare-earth intermetallics. *Comput. Mater. Sci.* **2014**, *90*, 56–60. [CrossRef]
29. De Luca, A.; Shu, S.; Seidman, D. Effect of microadditions of Mn and Mo on dual $L1_2$- and α-precipitation in a dilute Al-Zr-Sc-Er-Si alloy. *Mater. Charact.* **2020**, *169*, 110585. [CrossRef]
30. De Luca, A.; Seidman, D.; Dunand, D. Mn and Mo additions to a dilute Al-Zr-Sc-Er-Si-based alloy to improve creep resistance through solid-solution- and precipitation-strengthening. *Acta Mater.* **2020**, *194*, 60–67. [CrossRef]
31. Farkoosh, A.; Dunand, D.; Seidman, D. Tungsten solubility in $L1_2$-ordered $Al_3Er$ and $Al_3Zr$ nanoprecipitates formed by aging in an aluminum matrix. *J. Alloys Compd.* **2020**, *820*, 153383. [CrossRef]
32. Özer, T. Study of First Principles on Anisotropy and Elastic Constants of $YAl_3$ Compound. *Can. J. Phys.* **2019**, *98*, 357–363. [CrossRef]
33. Michi, R.A.; Perrin Toinin, J.; Farkoosh, A.R.; Seidman, D.N.; Dunand, D.C. Effects of Zn and Cr additions on precipitation and creep behavior of a dilute Al–Zr–Er–Si alloy. *Acta Mater.* **2019**, *181*, 249–261. [CrossRef]
34. Dorin, T.; Babaniaris, S.; Jiang, L.; Cassel, A.; Robson, J.D. Stability and stoichiometry of $L1_2$ $Al_3$(Sc,Zr) dispersoids in Al-(Si)-Sc-Zr alloys. *Acta Mater.* **2021**, *216*, 117117. [CrossRef]
35. Henderson, H.B.; Hammons, J.A.; Baker, A.A.; McCall, S.K.; Li, T.T.; Perron, A.; Sims, Z.C.; Ott, R.T.; Meng, F.; Thompson, M.J.; et al. Enhanced thermal coarsening resistance in a nanostructured aluminum-cerium alloy produced by additive manufacturing. *Mater. Des.* **2021**, *209*, 109988. [CrossRef]
36. Hung, C.J.; Nayak, S.K.; Sun, Y.; Fennessy, C.; Vedula, V.K.; Tulyani, S.; Lee, S.-W.; Alpay, S.P.; Hebert, R.J. Novel Al-X alloys with improved hardness. *Mater. Des.* **2020**, *192*, 108699. [CrossRef]
37. Liu, S.H.; Wang, G.Q.; Min, W.A.; Gao, H.W.; Mao, L.C. Effects of rare earth elements on electrical conductivity of industrial aluminum. *Chin. J. Nonferrous Met.* **2000**, *10*, 335.
38. Timpel, M.; Wanderka, N.; Murty, B.S.; Banhart, J. Three-dimensional visualization of the microstructure development of Sr-modified Al–15Si casting alloy using FIB-EsB tomography. *Acta Mater.* **2010**, *58*, 6600–6608. [CrossRef]
39. Choi, S.W.; Kim, Y.M.; Lee, K.M.; Cho, H.S.; Hong, S.K.; Kim, Y.C.; Kang, C.S.; Kumai, S. The effects of cooling rate and heat treatment on mechanical and thermal characteristics of Al–Si–Cu–Mg foundry alloys. *J. Alloys Compd.* **2014**, *617*, 654–659. [CrossRef]
40. García-García, G.; Espinoza-Cuadra, J.; Mancha-Molinar, H. Copper content and cooling rate effects over second phase particles behavior in industrial aluminum–silicon alloy 319—ScienceDirect. *Mater. Des.* **2007**, *28*, 428–433. [CrossRef]
41. Marquis, E.A.; Seidman, D.N. Nanoscale structural evolution of $Al_3Sc$ precipitates in Al(Sc) alloys. *Acta Mater.* **2001**, *49*, 1909–1919. [CrossRef]
42. Woodward, C.; Asta, M.; Kresse, G.; Hafner, J. Density of constitutional and thermal point defects in $L1_2$-$Al_3Sc$. *Phys. Rev. B* **2001**, *63*, 094103. [CrossRef]
43. Fu, C.L. Electronic, elastic, and fracture properties of trialuminide alloys: $Al_3Sc$ and $Al_3Ti$. *J. Mater. Res.* **1990**, *5*, 971–979. [CrossRef]
44. Clouet, E.; Nastar, M.; Sigli, C. Nucleation of $Al_3Zr$ and $Al_3Sc$ in aluminum alloys: From kinetic Monte Carlo simulations to classical theory. *Phys. Rev. B* **2004**, *69*, 064109. [CrossRef]
45. Fu, L.; Ke, J.L.; Zhang, Q.; Tang, B.Y.; Peng, L.M.; Ding, W.J. Mechanical properties of $L1_2$ type $Al_3X$ (X = Mg, Sc, Zr) from first-principles study. *Phys. Status Solidi B* **2012**, *249*, 1510–1516. [CrossRef]

46. Colinet, C.; Pasturel, A.; Manh, D.N.; Pettifor, D.; Miodownik, P. Phase-stability study of the Al-Nb system. *Phys. Rev. B* **1997**, *56*, 552. [CrossRef]
47. Chen, Z.; Zhang, P.; Chen, D.; Wu, Y.; Wang, M.; Ma, N.; Wang, H. First-principles investigation of thermodynamic, elastic and electronic properties of $Al_3V$ and $Al_3Nb$ intermetallics under pressures. *J. Appl. Phys.* **2015**, *117*, 085904. [CrossRef]
48. Liu, T.; Ma, T.; Li, Y.; Ren, Y.; Liu, W. Stable, mechanical and thermodynamic properties of Al-RE intermetallics: A First-principles study. *J. Rare Earths* **2022**, *40*, 345–352. [CrossRef]
49. Lv, C.; Yang, J.; Zhang, X.; Cai, Y.; Liu, X.; Wang, G.; Luo, S.-N. Interfacial effect on deformation and failure of Al/Cu nanolaminates under shear loading. *J. Phys. D Appl. Phys.* **2018**, *51*, 335301. [CrossRef]
50. Zhao, S.; Stocks, G.M.; Zhang, Y. Stacking fault energies of face-centered cubic concentrated solid solution alloys. *Acta Mater.* **2017**, *134*, 334–345. [CrossRef]
51. Chowdhury, P.; Sehitoglu, H. Deformation physics of shape memory alloys–Fundamentals at atomistic frontier. *Prog. Mater. Sci.* **2017**, *88*, 49–88. [CrossRef]
52. Van Swygenhoven, H.; Derlet, P.M.; Froseth, A.G. Stacking fault energies and slip in nanocrystalline metals. *Nat. Mater.* **2004**, *3*, 399–403. [CrossRef]
53. Fan, T.W.; Wang, Z.P.; Lin, J.J.; Chen, D.C.; Fang, Q.H.; Hu, T.; Nie, B.H.; Wang, K.; Hu, H.W.; Sun, H.B.; et al. First-principles predictions for stabilizations of multilayer nanotwins in Al alloys at finite temperatures. *J. Alloys Compd.* **2019**, *783*, 765–771. [CrossRef]
54. Zhou, W.; Ren, X.; Ren, Y.; Yuan, S.; Ren, N.; Yang, X.; Adu-Gyamfi, S. Initial dislocation density effect on strain hardening in FCC aluminium alloy under laser shock peening. *Philos. Mag.* **2017**, *97*, 1–13. [CrossRef]
55. Hui, J.; Zhang, X.; Liu, T.; Liu, W.; Wang, B. First-principles calculation of twin boundary energy and strength/embrittlement in hexagonal close-packed titanium. *Mater. Des.* **2022**, *213*, 110331. [CrossRef]
56. Yan, H.; Guo, W.; Luan, T.; Ma, X.; Xu, G.; Leng, X.; Zhao, W.; Yan, J. Strengthening mechanism of Al/Sn interfaces: Study from experiments and first-principles calculation. *Mater. Des.* **2021**, *212*, 110292. [CrossRef]
57. Zhang, X.; Huang, Y.; Liu, Y.; Ren, X. A comprehensive DFT study on the thermodynamic and mechanical properties of $L1_2$-$Al_3Ti$/Al interface. *Vacuum* **2021**, *183*, 109858. [CrossRef]
58. Jiang, D.; Xiao, W.; Liu, D.; Liu, S. Structural stability, electronic structures, mechanical properties and debye temperature of W-Re alloys: A first-principles study. *Fusion Eng. Des.* **2020**, *162*, 112081. [CrossRef]
59. Maruhn, J.A.; Reinhard, P.G.; Suraud, E. *Density Functional Theory*; Plenum Press: New York, NY, USA, 2010.
60. Perdew, J.P.; Burke, K.; Ernzerhof, M. Generalized Gradient Approximation Made Simple. *Phys. Rev. Lett.* **1996**, *77*, 3865–3868. [CrossRef] [PubMed]
61. Hafner, J. Ab-initio simulations of materials using VASP: Density-functional theory and beyond. *J. Comput. Chem.* **2008**, *29*, 2044–2078. [CrossRef]
62. Kresse, G.; Joubert, D. From ultrasoft pseudopotentials to the projector augmented-wave method. *Phys. Rev. B* **1999**, *59*, 1758–1775. [CrossRef]
63. Monkhorst, H.J.; Pack, J.D. Special points for Brillouin-zone integrations. *Phys. Rev. B* **1976**, *13*, 5188–5192. [CrossRef]
64. Feynman, R.P. Forces in Molecules. *Phys. Rev.* **1939**, *56*, 340. [CrossRef]
65. Wang, V.; Xu, N.; Liu, J.; Tang, G.; Geng, W. VASPKIT: A User-friendly Interface Facilitating High-throughput Computing and Analysis Using VASP Code. *Comput. Phys. Commun.* **2021**, *267*, 108033. [CrossRef]
66. Madsen, G.; Carrete, J.; Verstraete, M.J. BoltzTraP2, a program for interpolating band structures and calculating semi-classical transport coefficients. *Comput. Phys. Commun.* **2018**, *231*, 140–145. [CrossRef]
67. Zhang, S.; Northrup, J. Chemical potential dependence of defect formation energies in GaAs: Application to Ga self-diffusion. *Phys. Rev. Lett.* **1991**, *67*, 2339. [CrossRef] [PubMed]
68. Dong, T.; Zhang, X.; Yang, L.; Wang, F. An effect of structural vacancies on the lattice vibration, mechanical, electronic and thermodynamic properties of $Cr_5BSi_3$. *Chin. Phys. B* **2021**, *31*, 026101. [CrossRef]
69. Qiu, R.; Lu, H.; Ao, B.; Huang, L.; Tang, T.; Chen, P. Energetics of intrinsic point defects in aluminium via orbital-free density functional theory. *Philos. Mag.* **2017**, *97*, 2164–2181. [CrossRef]
70. Bandyopadhyay, J.; Gupta, K.P. Low temperature lattice parameters of Al and Al-Zn alloys and Grüneisen parameter of Al. *Cryogenics* **1978**, *18*, 54–55. [CrossRef]
71. Ehrhart, P. *Atomic Defects in Metals*; Ullmaier, H., Ed.; Springer: Berlin/Heidelberg, Germany, 1991; Volume 25.
72. Carling, K.; Wahnström, G.; Mattsson, T.R.; Mattsson, A.E.; Sandberg, N.; Grimvall, G. Vacancies in Metals: From First-Principles Calculations to Experimental Data. *Phys. Rev. Lett.* **2000**, *85*, 3862. [CrossRef]
73. Fujikawa, S.I.; Sugaya, M.; Takei, H.; Hirano, K.I. Solid solubility and residual resistivity of scandium in aluminum. *J. Less-Common Met.* **1979**, *63*, 87–97. [CrossRef]
74. Van De Walle, A.; Ceder, G. The effect of lattice vibrations on substitutional alloy thermodynamics. *Rev. Mod. Phys.* **2002**, *74*, 11. [CrossRef]
75. Ravindran, P.; Fast, L.; Korzhavyi, P.A.; Johansson, B.; Wills, J.; Eriksson, O. Density functional theory for calculation of elastic properties of orthorhombic crystals: Application to $TiSi_2$. *J. Appl. Phys.* **1998**, *84*, 4891–4904. [CrossRef]
76. Page, Y.L.; Saxe, P. Symmetry-general least-squares extraction of elastic coefficients fromab initiototal energy calculations. *Phys. Rev. B* **2001**, *63*, 174103. [CrossRef]

77. Sergio, G.V.; Alonso, J.A.; Gonzalo, S.; Martínez, J. Structure, stability, and optical absorption spectra of small $Ti_nC_x$ clusters: A first-principles approach. *Mon. Not. R. Astron. Soc.* **2021**, *508*, 5074–5091.
78. Wang, M.; Xie, J.; Xue, K.; Li, L. First-principles study of high-pressure structural stability and mechanical properties of $Ni_2B$. *Comput. Mater. Sci.* **2021**, *194*, 110465. [CrossRef]
79. Li, C.; Wang, Z. First-principles study of structural, electronic, and mechanical properties of the nanolaminate compound $Ti_4GeC_3$ under pressure. *J. Appl. Phys.* **2010**, *107*, 201. [CrossRef]
80. Hao, A.; Yang, X.; Wang, X.; Zhu, Y.; Liu, X.; Liu, R. First-principles investigations on electronic, elastic and optical properties of XC (X = Si, Ge, and Sn) under high pressure. *J. Appl. Phys.* **2010**, *108*, 9. [CrossRef]
81. Chen, X.-Q.; Niu, H.; Li, D.; Li, Y. Modeling hardness of polycrystalline materials and bulk metallic glasses. *Intermetallics* **2011**, *19*, 1275–1281. [CrossRef]
82. Wang, Y.; Meng, Y.; Wang, J.; Zhang, C.; Huang, H. Mechanical properties of defective $L1_2$-$Al_3X$ (X = Sc, Lu) phase: A first-principle study. *J. Rare Earths* **2020**, *39*, 217–224. [CrossRef]
83. Gu, Q.; Ji, J.; Guo, F.; Chen, H.; Yang, T.; Tan, X. First Principle Study on the Electronic, Magnetic and Phase Stability of the Full-Heusler Compound $Fe_2CuSi$. *SPIN* **2021**, *11*, 2150001. [CrossRef]
84. Pu, Y.; Qiu, Z.; Lv, B.; Fang, C.; Lou, Y.; Wang, W.; Dai, Q. The first-principle study on certain structural, band-structural, elastic, optical and piezoelectric properties of the Ca, Zr and Ca/Zr-doped $BaTiO_3$. *Mod. Phys. Lett. B* **2023**, *37*, 2350007. [CrossRef]
85. Mebed, A.M.; Ali, M.A. First-principles calculations to investigate structural, elastic, electronic and thermoelectric properties of narrow-band gap half-Heusler RhVX(X = Si, Ge) compounds. *Int. J. Mod. Phys. B* **2023**, *37*, 22350163. [CrossRef]
86. Meng, B.; Jing, T.; Xiao, W.Z. First-principle study on the stability, mechanical, electronic, and optical properties of two-dimensional scandium oxyhalides. *Mater. Chem. Phys.* **2022**, *287*, 126306. [CrossRef]
87. Deng, Y.; Jia, O.H.; Chen, X.R.; Zhu, J. Phase transition and elastic constants of CaO from first-principle calculations. *Phys. B* **2007**, *392*, 229–232. [CrossRef]
88. Wei, J.; Zhang, L.; Liu, Y. First-principles calculations study the mechanical and thermal properties of Cr–Al–B ternary borides. *Solid State Commun.* **2021**, *326*, 114182. [CrossRef]
89. Chen, C.; Fan, S.; Niu, J.; Huang, H.; Yuan, G. Alloying design strategy for biodegradable zinc alloys based on first-principles study of solid solution strengthening. *Mater. Des.* **2021**, *204*, 109676. [CrossRef]
90. Pettifor, D.G. Theoretical predictions of structure and related properties of intermetallics. *Mater. Sci. Technol.* **1992**, *8*, 345–349. [CrossRef]
91. Wallace, D.C. Thermodynamics of crystals. *Am. J. Phys.* **1972**, *40*, 1718–1719. [CrossRef]
92. Johnson, R.A. Analytic nearest-neighbor model for fcc metals. *Phys. Rev. B* **1988**, *37*, 3924–3931. [CrossRef]
93. Fu, H.; Zhao, Z.; Liu, W.; Peng, F.; Gao, T.; Cheng, X. Ab initio calculations of elastic constants and thermodynamic properties of γ-TiAl under high pressures. *Intermetallics* **2010**, *18*, 761–766. [CrossRef]
94. Frantsevich, I.N.; Voronov, F.F.; Bokuta, S.A. *Elastic Constants and Elastic Moduli of Metals and Insulators Handbook*; Naukova Dumka: Kiev, Ukraine, 1983.
95. Mallick, P.K. *Materials, Design and Manufacturing for Lightweight Vehicles*; CRC Press: Boca Raton, FL, USA, 2010.
96. Takahashi, K.; Kuwahara, H.; Kawasaki, N.; Obata, T.; Sugawa, E. Enhancement of Thermal Contact Conductance Between Metal Surfaces in an Induction Motor. *J Enhanc. Heat Transf.* **2001**, *8*, 201–213. [CrossRef]
97. Powell, R.W. Correlation of metallic thermal and electrical conductivities for both solid and liquid phases. *Int. J. Heat Mass Transfer* **1965**, *8*, 1033–1045. [CrossRef]
98. Madsen, G.; Singh, D.J. BoltzTraP. A code for calculating band-structure dependent quantities. *Comput. Phys. Commun.* **2006**, *175*, 67–71. [CrossRef]
99. Yadav, M.K.; Sanyal, B. First principles study of thermoelectric properties of Li-based half-Heusler alloys. *J. Alloys Compd.* **2015**, *622*, 388–393. [CrossRef]
100. Mubashir, S.; Butt, M.K.; Yaseen, M.; Iqbal, J.; Laref, A. Pressure induced electronic, optical and thermoelectric properties of cubic BaZrO3: A first principle calculations. *Opt. Int. J. Light Electron Opt.* **2021**, *239*, 166694. [CrossRef]
101. Remil, G.; Zitouni, A.; Bouadjemi, B.; Houari, M.; Bentata, S. A potential full Heusler thermoelectric material $CO_2ZrZ$ (Z = Al, Si, Ga and Sn) in low temperature: An Ab-initio investigation. *Solid State Commun.* **2021**, *336*, 114422. [CrossRef]
102. Wen, B.; Feng, X. Thermal conductivity of metal from first principles calculations and its application in aluminum. *J. Yanshan Univ.* **2015**, *39*, 298–306.
103. Brandt, R.; Neuer, G. Electrical Resistivity and Thermal Conductivity of Pure Aluminum and Aluminum Alloys up to and above the Melting Temperature. *Int. J. Thermophys.* **2007**, *28*, 1429–1446. [CrossRef]


**Disclaimer/Publisher's Note:** The statements, opinions and data contained in all publications are solely those of the individual author(s) and contributor(s) and not of MDPI and/or the editor(s). MDPI and/or the editor(s) disclaim responsibility for any injury to people or property resulting from any ideas, methods, instructions or products referred to in the content.